Lifetime statistics for a Bloch particle in ac and dc fields

M. Glück, A. R. Kolovsky,* and H. J. Korsch
Fachbereich Physik, Universität Kaiserslautern, D-67653 Kaiserslautern, Germany
(Received 16 December 1998)

We study the statistics of the Wigner delay time and resonance width for a Bloch particle in ac and dc fields in the regime of quantum chaos. It is shown that after appropriate rescaling the distributions of these quantities have a universal character predicted by the random matrix theory of chaotic scattering.
[S1063-651X(99)09907-9]

PACS number(s): 05.45.−a, 03.65.−w, 73.20.Dx

I. INTRODUCTION

Chaotic scattering has been a subject of rather intensive research activity during the last decade (see Refs. [1–3], and references therein). This phenomenon is encountered in a variety of physical systems ranging from nuclei, atoms, and molecules, to mesoscopic ballistic devices and microwave cavities. In this paper we report the results of our study on chaotic scattering of a Bloch particle (a particle in a periodic potential) in the presence of a constant force and a time-periodic driving. That is, we consider a system with the Hamiltonians

$$H = H_0 + Fx + F_\omega x \cos(\omega t), \tag{1}$$

$$H_0 = p^2/2 + V(x), \tag{2}$$

where $V(x)$ is a periodic potential and, to be concrete, we choose $V(x) = \cos x$. The role of the external forces in Hamiltonian (1) is different: the periodic force typically make the system (classically) chaotic, while the constant force ''opens'' the system and requires a scattering approach for analyzing it. We present some results of the classical analysis of the system in Sec. II.

It should be noted that in this paper we use dimensionless variables, where the coordinate is measured in units of the space period of the potential and the time in periods of small particle oscillations near the bottom of the cosine potential. This scaling removes all parameters of the initial classical Hamiltonian (2). The quantum Hamiltonian (2), however, contains as a parameter the scaled Planck constant $\hbar'$, which enters the momentum operator ($p \to \hat{p} = -i\hbar' d/dx$). If V_0 is the amplitude of the periodic potential in the unscaled Hamiltonian, a its space period, and M the particle mass, then the scaled Planck constant $\hbar' = 2\pi\hbar/a(MV_0)^{1/2}$. In what follows we omit the prime, i.e., $\hbar$ in the paper always denote the *scaled* Planck constant.

The quantum analysis of system (1) is essentially more subtle. It need not to be mentioned that the Hamiltonian (1) corresponds to a one-dimensional model of a crystal electron in a static and periodic electric fields. Being very physically important, this model has attracted much attention since the early days of quantum mechanics. Usually the analysis is performed by using specific tools of quantum mechanics, without any reference to the classical dynamics. This was actually justified, because the system parameters in the case of crystal electrons correspond to a deep quantum region. The situation has changed recently due to experiments with semiconductor superlattices [4] and, especially, due to experiments with neutral atoms in optical lattices [5–8]. For these systems the lattice period exceeds that in solid crystals by several orders, and the semiclassical region becomes accessible. It is understood that chaotic scattering (which is the topic of the present paper) implies a semiclassical region of the parameters. In the notation used, this means that the dimensionless Planck constant (entering the momentum operator) is less than unity.

The simplest approach in a quantum-mechanical analysis of system (1) involves the so-called single-band approximation, i.e., one keeps in consideration only one Bloch band from the whole energy spectrum of the initial Hamiltonian (2). In this way we immediately come to a fundamental notion of the Bloch period $T_B = \hbar/F$, which is a pure quantum quantity. The appearance of a new time period involves the other important characteristic of the system — the condition of commensurability between the Bloch period T_B and the period $T_\omega = 2\pi/\omega$ of the driving force. The properties of system (1) in a single-band approximation were studied in Refs. [9]. It should be realized, however, that a single-band (more generally, an N band) approximation effectively ''closes'' the system [10]. In fact, the physical mechanism that makes the system ''open'' is the Landau-Zenner tunneling between the adjacent bands. Correctly taking into account the interband transition is a rather complicated problem, which has been discussed for years (see Ref. [11], for example). In Sec. III we describe an approach which overcomes this problem and ensures a system analysis without any approximation [12,13]. We introduce the notion of an effective scattering matrix for system (1), and identify the number of scattering channels with the dominator q of the commensurability condition $T_B/T_\omega = r/q$ (r,q are coprime integers).

The results of a numerical analysis of the system are presented in Sec. IV. We restrict ourselves to calculating the complex poles of the scattering matrix, i.e., resonances, and the Wigner delay time (the definition of this quantity, characterizing the continuous quasienergy spectrum of the system, is given in Sec. IV). In addition, we consider only the

*Also at L. V. Kirensky Institute of Physics, 660036 Krasnoyarsk, Russia.

case of a small number of channels, which is very interesting because of the strong deviation between the quantum and classical dynamics [14,15]. In fact, although the system itself is assumed to be semiclassical ($\hbar<1$), a small number q of open channels makes it behave quantum-mechanically. (To avoid a misunderstanding, we stress that the term ''semiclassical'' refers here only the condition $\hbar<1$. It should not be mismatched with the condition $q\gg1$, which is often referred to as the semiclassical regime in the theory of chaotic scattering.)

The main issue we discuss in this paper is the statistics of the Wigner delay times and resonance widths. It is shown that after an appropriate rescaling, the distributions for these quantities have a universal character. The calculated distributions will then be compared with the prediction of random matrix theory (RMT), thus providing both a test for this abstract theory and a deeper understanding of the features of system (1).

The random matrix approach is a powerful analytical method in the field of quantum chaos, including chaotic scattering. It is based on the famous conjecture that in the case of chaotic classical dynamics the quantum Hamiltonian can be modeled by a random matrix sharing the same symmetry. General expressions for the statistics of many quantities (like delay time or resonance width) were obtained for the case of a Gaussian ensemble of random matrices (see Ref. [16], and references therein). We recall some of the known results in Sec. V. Then we define a different (from the commonly used) random scattering matrix. It is based on the circular ensemble instead of the Gaussian one, and is an appropriate random scattering matrix for modeling our system of interest. A numerical comparison between the statistics drawn from two different definitions of the random scattering matrices allows us to identify the analytical expressions for the distribution of the resonance width and delay time, against which the result of Sec. IV should be compared.

This comparison is given in Sec. VI. We show that the statistics of the Wigner delay time fits the analytical formula rather well. The statistics of the resonance width also qualitatively coincides with the prediction of RMT. We also study the different symmetries of the Hamiltonian. In fact, it is well known that the prediction of RMT crucially depends on the symmetry class — orthogonal, unitary, or symplectic. It is argued in this paper that the appropriate random matrix ensemble for modeling the properties of system (1) is the circular unitary ensemble (CUE). In Sec. VI we briefly consider another dynamical system, which classically has essentially the same dynamics, but possesses a higher symmetry in the quantum case. We show that the difference between two symmetry classes can be well observed in statistics of the Wigner delay time.

II. CLASSICAL DYNAMICS

It is convenient to include the time-periodic term in Hamiltonian (1) in Hamiltonian (2), which is done by the canonical transformations $p\to p+(F_\omega/\omega)\sin(\omega t)$ and $x\to x-(F_\omega/\omega^2)\cos(\omega t)$. Then the system Hamiltonian takes the form

$$H=\frac{p^2}{2}+V(x,t)+Fx, \tag{3}$$

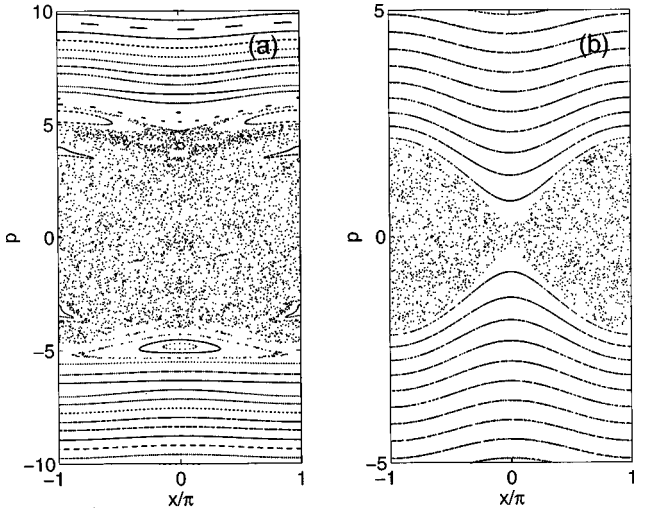

FIG. 1. (a) Phase portrait of system (3) and (4) for $F=0$, $\omega=\frac{10}{6}$, and $\epsilon=1.5$. (b) Phase portrait of system (7) for $F=0$ and $\omega=0.3$.

where

$$V(x,t)=\cos[x-\epsilon\cos(\omega t)],\quad \epsilon=\frac{F_\omega}{\omega^2}. \tag{4}$$

It is also useful to expand the ''new'' time-dependent potential $V(x,t)$ in the Fourier series

$$V(x,t)=J_0(\epsilon)\cos x+\sum_{m=1}^{\infty}J_m(\epsilon)[\cos(x-m\omega t)+(-1)^m\cos(x+m\omega t)], \tag{5}$$

where $J_m(\epsilon)$ are the Bessel functions. It follows from Eq. (5) that for $F=0$ the system (3) is a system of many interacting nonlinear resonances and, therefore, its dynamics can be either quasiregular or chaotic depending on a particular choice of the parameters ω and ϵ [17]. Here we restrict ourselves to the same choices $\omega=10/6$ and $\epsilon=1.5$ as in the experiment [6], where a developed chaos exists [see Fig. 1(a)].

Assume now that $F>0$, and that the initial momentum of the particle well exceeds the value $p^*\approx5$ corresponding to the boundary between the chaotic and regular components in Fig. 1(a). Then the scattering process consists of three stages: almost uniformly deaccelerated motion for $p>p^*$, temporal chaotic motion for $|p|<p^*$, and accelerated motion for $p<-p^*$ (see Fig. 2). The time spent by the particle in chaotic region is determined by the delay time, and varies randomly with the initial condition. We define the classical delay time τ as the time gain or loss relative the case $V(x,t)\equiv0$. Figure 3 shows the distribution $P_{\rm cl}(\tau)$ of the classical delay time for $F=0.065$. It is seen that the distribution has an exponential tail

$$P_{\rm cl}(\tau)\sim\exp(-\tau/\tau^*), \tag{6}$$

which is the ''trademark'' of the chaotic scattering. The value of the decay increment τ^* primarily depends on F, and for $F=0.13$ and $F=0.065$ (used later on in the quantum simulation) is $\tau^*\approx0.13F$ and $\tau^*\approx0.20F$, respectively.

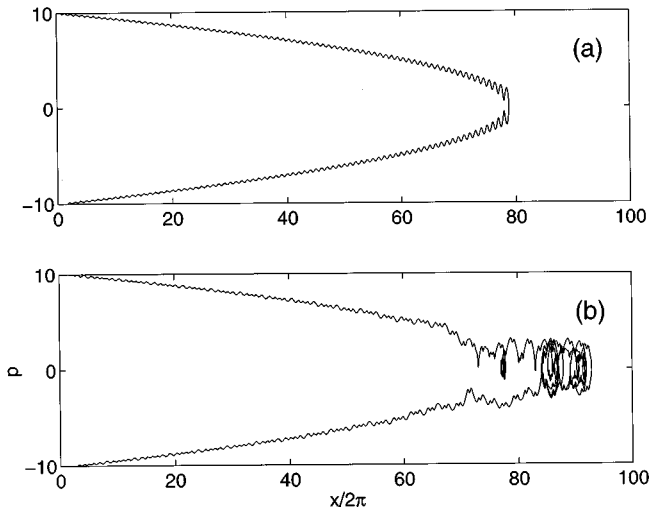

FIG. 2. Example of a classical trajectory for system (3) and (4) for $F=0.13$, $\epsilon=0$ (a), and $\omega=\frac{10}{6}$, $\epsilon=1.5$ (b).

To conclude this section we note that the considered potential (4) is only one of the potentials which can be realized in experiments with optical lattices. In particular in Refs. [7,8] the potential $V(x,t)=f(\omega t)\cos x$ (periodic modulation of laser intensity) was used. The chaotic scattering by this potential is similar to that considered above. In Sec. VI we shall consider the Hamiltonian [18]

$$H=\frac{p^2}{2}+\cos(\omega t)\cos x+Fx. \tag{7}$$

The phase portrait for this system is shown in Fig. 1(b) for $F=0$ and $\omega=0.3$. From a theoretical viewpoint system (7) is preferable to system (1), because of the simpler structure of the classical phase space. In addition, it possesses a higher symmetry than system (1).

III. SCATTERING MATRIX

In this section we introduce the notion of an effective scattering matrix, which relates the asymptotic solution for a quantum particle coming from infinity and scattered back to infinity [13]. The key differences between our approach and the common approach of scattering theory are that the analysis is done in momentum space, and that we consider the system evolution operator instead of the system Hamiltonian.

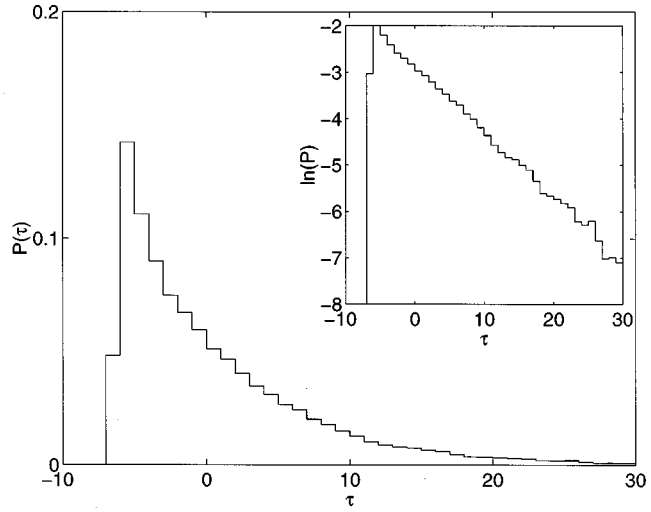

FIG. 3. Distribution of the scaled ($\tau\rightarrow F\tau$) classical delay time. The parameters are $F=0.065$, $\epsilon=1.5$, and $\omega=10/6$.

A. Floquet operator

We shall describe the quantum dynamics of the system with the help of the evolution operator $\hat{U}(t)$. In what follows we assume the commensurability condition

$$rT_\omega=qT_B=T. \tag{8}$$

[The incommensurate case can then be approached through the limit $r,q\rightarrow\infty, r/q\rightarrow$ (irrational).] It is proved in Ref. [12] that — provided the condition (8) is satisfied — system evolution operator possesses the property

$$\hat{U}(nT)=\hat{U}^n(T), \tag{9}$$

and, thus, we can focus on studying the spectral properties of the time-Floquet operator [i.e., the evolution operator $\hat{U}(T)$ over the period T]:

$$\hat{U}(T)\psi(x)=\exp(-i\lambda)\psi(x). \tag{10}$$

We obtain an explicit expression for $\hat{U}(T)$ by using the standard substitution $\psi(x,t)=\exp(-iFtx/\hbar)\tilde{\psi}(x,t)$ in the Schrödinger equation, which eliminates the static term in Hamiltonian (3). Then

$$\hat{U}(T)=e^{-iqx}\hat{W}, \tag{11}$$

where

$$\hat{W}=\widehat{\exp}\left\{-\frac{i}{\hbar}\int_0^T\left[\frac{(\hat{p}-Ft)^2}{2}+V(x,t)\right]dt\right\}, \tag{12}$$

and the caret over the exponent denotes time ordering. It is seen from Eqs. (11) and (12) that the evolution operator commutes with the translational operator over the lattice period and, therefore, the quasimomentum k is a good quantum number. Presenting the wave function in Eq. (10) in the form

$$\psi(x)=e^{ikx}\sum_{n=-\infty}^{\infty}c_n^{(k,\lambda)}\langle x|n\rangle, \quad \langle x|n\rangle=(2\pi)^{-1/2}e^{inx}, \tag{13}$$

we reduce the eigenvalue problem (10) to the diagonalization of an infinite matrix given by the product of two unitary matrices:

$$QW^{(k)}\mathbf{c}^{(k,\lambda)}=\exp(-i\lambda)\mathbf{c}^{(k,\lambda)}. \tag{14}$$

In Eq. (14), Q is the shift matrix with the elements

$$Q_{n',n}=\langle n'|\exp(-iqx)|n\rangle=\delta_{n',n-q}, \tag{15}$$

and the elements of the matrix $W^{(k)}$ are given by

$$W^{(k)}_{n',n}=\langle n'|\exp(-ikx)\hat{W}\exp(ikx)|n\rangle$$
$$=\langle n'|\widehat{\exp}\left\{-\frac{i}{\hbar}\int_0^T\left[\frac{(\hat{p}-Ft+\hbar k)^2}{2}+V(x,t)\right]dt\right\}|n\rangle. \quad (16)$$

By convention, the expansion coefficients $c_n^{(k,\lambda)}$ are arranged in a column vector $\mathbf{c}^{(k,\lambda)}$ with an index n decreasing from up to down.

We note that quasimomentum k enters Eq. (14) as a parameter. For a general $V(x,t)$ we should scan over $k(-\frac{1}{2}\leqslant k<\frac{1}{2})$ to obtain the whole spectrum. Excluded is the case of a time independent potential $V(x,t)=V(x)$. In this case the matrices $QW^{(k)}$ are unitarily equivalent and, therefore, the spectrum is degenerate [12]. In what follows, to simplify the formulas, we shall omit the quasimomentum index k and the quasienergy index λ.

B. Scattering matrix, $q=1$

First we consider the case $q=1$. The method of solving Eq. (14) is based on the fact that the matrix W tends asymptotically to a diagonal one:

$$W_{n',n}\to\delta_{n',n}w_n, \quad n,n'\to\pm\infty,$$
$$w_n=\exp\left[-\frac{i}{2\hbar}\int_0^T(\hbar n+\hbar k-Ft)^2\mathrm{d}t\right]. \quad (17)$$

Let us assume that the asymptotic (17) is satisfied ''good enough'' for $|n|>N$. Then we decompose the vector $\mathbf{c}$ into three subvectors

$$\mathbf{c}=\begin{pmatrix}\mathbf{c}^{(+)}\\ \mathbf{c}^{(0)}\\ \mathbf{c}^{(-)}\end{pmatrix}, \quad (18)$$

where $\mathbf{c}^{(+)}$ consists of the coefficients c_n with indices $n>N$, $\mathbf{c}^{(-)}$ with $n<-(N+1)$, and $\mathbf{c}^{(0)}$ is constructed from c_n with indices $-(N+1)\leqslant n\leqslant N$. The vector $\mathbf{c}^{(+)}$ is completely specified by the value of the coefficient c_{N+1} and the equation

$$w_nc_n=\exp(-i\lambda)c_{n-1}, \quad (19)$$

which follows from Eq. (14) for $q=1$ and the asymptotic (17). Analogously, the vector $\mathbf{c}^{(-)}$ is specified by Eq. (19) and the value of c_{-N-1}. For the vector $\mathbf{c}^{(0)}$ we have an algebraic equation

$$[B_N-\exp(-i\lambda)]\mathbf{c}^{(0)}=-w_{N+1}c_{N+1}\mathbf{e}_N. \quad (20)$$

Here B_N is a matrix of the structure

$$B_N=\begin{pmatrix}\mathbf{0} & 0\\ W_N & \mathbf{0}'\end{pmatrix}, \quad (21)$$

where W_N is the matrix W truncated to the size $(2N+1)(2N+1)$, $\mathbf{0}$ and $\mathbf{0}'$ are zero row and column vectors of the length $2N+1$, and $\mathbf{e}_N$ is a column vector of the size $2N+2$ with all elements equal to zero except the first one which is equal to unity. We note that Eq. (20) actually relates the coefficient c_{-N-1} to the coefficient c_{N+1} and, thus, matches two asymptotic solutions $\mathbf{c}^{(+)}$ and $\mathbf{c}^{(-)}$. Without loss of generality we can choose the phase of c_{N+1} such that $-w_{N+1}c_{N+1}=1$.

We define the matrix $G(\lambda)$ (of dimension 1×1 in the considered case $q=1$) as a phase gain (loss) relative to the case when the matrix W is given by Eq. (17) for arbitrary n and n' (we shall refer to the latter case as ''zero solution''). Thus

$$c_{-N-1}=G(\lambda)\tilde{c}_{-N-1}, \quad (22)$$

where $\tilde{c}_{-N-1}\sim\exp[i(2N+2)\lambda]$ is the zero solution. Using Eq. (20), the matrix $G(\lambda)$ can be presented in the form

$$G(\lambda)=\lim_{N\to\infty}a_N(\lambda)\mathbf{e}'_N[B_N-\exp(-i\lambda)]^{-1}\mathbf{e}_N, \quad (23)$$

where $\mathbf{e}'_N$ is a row vector with all elements equal to zero except the last one which is equal to unity, and the phase factor $a_N(\lambda)=\tilde{c}^*_{-N-1}$ is given by the zero solution. We also add the limit $N\to\infty$ in Eq. (23), which ensures the validity of the asymptotic formula (17). The numerical calculation of the scattering matrix (23) indicates a rapid convergence for the limit.

C. Scattering matrix, arbitrary q

For arbitrary q, Eq. (19) has the form

$$w_nc_n=\exp(-i\lambda)c_{n-q}. \quad (24)$$

It follows from Eq. (24) that there are q independent solutions $\mathbf{c}^{(\pm,i)}$, $(i=1,\ldots,q)$, and, therefore, the matrix $G(\lambda)$ is of dimension $q\times q$. We adopt Eq. (23) for this case by substituting the vectors $\mathbf{e}_N$ and $\mathbf{e}'_N$ by a $q\times(2N+1+q)$ matrix e_N and a $(2N+1+q)\times q$ matrix e'_N of the following structure (shown for $q=2$ and $N=2$):

$$e_N=\begin{pmatrix}1&0\\0&1\\0&0\\0&0\\0&0\\0&0\\0&0\end{pmatrix}, \quad e'_N=\begin{pmatrix}0&0&0&0&0&1&0\\0&0&0&0&0&0&1\end{pmatrix}. \quad (25)$$

The prefactor a_N is a diagonal $q\times q$ matrix with elements given by the zero solutions. In Eq. (21), defining the matrix B_N, the zero vectors should also be substituted for by zero matrices. Below we give a proof that the matrix $G(\lambda)$ constructed this way is explicitly unitary, i.e., $G^+G=\hat{1}$.

First we prove the statement for the matrix $G(\lambda)$ defined as

$$G(\lambda)=e'[B-\exp(-i\lambda)]^{-1}e, \quad (26)$$

$$B=\begin{pmatrix} 0_{M\times N} & 0_{M\times M} \\ A & 0_{N\times M} \end{pmatrix}, \tag{27}$$

where $A=A_{N\times N}$ is an arbitrary unitary matrix, and the matrices $e'=e'_{M\times(N+M)}$ and $e=e_{(N+M)\times M}$ have the same structure as in the example Eq. (25). (We note that here we change the notations as $q\to M$ and $2N+1\to N$. This is done for the sake of comparison with results of Sec. V). From Eq. (26) we see that the columns of the matrix $G(\lambda)$ are formed by the last M elements of the vectors $\mathbf{c}^i$ satisfying the equation

$$(B-e^{-i\lambda})\mathbf{c}^i=\mathbf{e}^i \tag{28}$$

($\mathbf{e}^i$ is the ith column of the matrix e). Denoting the ith column of the matrix $G(\lambda)$ by $\mathbf{g}^i$, and presenting the vector $\mathbf{c}^i$ as

$$\mathbf{c}^i=\begin{pmatrix} \tilde{\mathbf{c}}^i \\ \mathbf{g}^i \end{pmatrix}, \tag{29}$$

we obtain from Eq. (28) that

$$\begin{pmatrix} 0_{1,M} \\ A\tilde{\mathbf{c}}^i \end{pmatrix}-\mathbf{e}^i=e^{-i\lambda}\begin{pmatrix} \tilde{\mathbf{c}}^i \\ \mathbf{g}^i \end{pmatrix}. \tag{30}$$

Now we take the scalar product of both vectors on the left and right hand sides of equality (30) with those for a different index j:

$$(A\tilde{\mathbf{c}}^i,A\tilde{\mathbf{c}}^j)+(\mathbf{e}^i,\mathbf{e}^j)=(\tilde{\mathbf{c}}^i,\tilde{\mathbf{c}}^j)+(\mathbf{g}^i,\mathbf{g}^j). \tag{31}$$

Because the matrix A is unitary and $(\mathbf{e}^i,\mathbf{e}^j)=\delta_{i,j}$, from Eq. (31) we obtain

$$(\mathbf{g}^i,\mathbf{g}^j)=\sum_{n=1}^{M} G^*_{n,i}G_{n,j}=\sum_{n=1}^{M} G^+_{i,n}G_{n,j}=\delta_{i,j}. \tag{32}$$

This ends the proof. The extension of this proof to the case of the scattering matrix for a Bloch particle is straightforward because for any finite N it is just the product of the matrix (26) with the diagonal unitary matrix constructed from the coefficients $a_N(\lambda)$.

Besides the relation to the problem currently discussed, the scattering matrix (26) is of its own interest. In Sec. V we shall use the construction of Eqs. (26) and (27) to define a random scattering matrix. For the purpose of future use we display one more useful relation, which defines the normalization of the vectors $\mathbf{c}^i$ in Eq. (28). Let us differentiate both side of Eq. (30) with respect to λ. We obtain

$$\begin{pmatrix} 0_{1,M} \\ A\partial_\lambda\tilde{\mathbf{c}}^i \end{pmatrix}=-ie^{-i\lambda}\mathbf{c}^i+e^{-i\lambda}\begin{pmatrix} \partial_\lambda\tilde{\mathbf{c}}^i \\ \partial_\lambda\mathbf{g}^i \end{pmatrix}, \tag{33}$$

where the subindex λ denotes the derivative. Taking the scalar product of Eq. (33) with Eq. (30), we have

$$(A\tilde{\mathbf{c}}^i,A\partial_\lambda\tilde{\mathbf{c}}^j)=-i(\mathbf{c}^i,\mathbf{c}^j)+(\tilde{\mathbf{c}}^i,\partial_\lambda\tilde{\mathbf{c}}^j)+(\mathbf{g}^i,\partial_\lambda\mathbf{g}^j), \tag{34}$$

or

$$(\mathbf{c}^i,\mathbf{c}^j)=-i\left(G^+\frac{dG}{d\lambda}\right)_{i,j}. \tag{35}$$

D. Complex poles of the scattering matrix

It follows from Eq. (23) that the poles of the scattering matrix $G(\lambda)$ (i.e., the resonances) are the eigenvalues z of the matrix B_N,

$$B_N\mathbf{c}=z\mathbf{c}. \tag{36}$$

We note that for any finite N the matrix B_N is *not* unitary and, thus, $|z|<1$. Altogether we have $2N+1-q$ nontrivial solutions of Eq. (36).

One can also take into account the formal limit $N\to\infty$ in Eq. (23). Then Eq. (36) transforms into the equation

$$QW\mathbf{c}=z\mathbf{c}, \tag{37}$$

accompanied by the non-Hermitian boundary condition

$$|c_n|\to 0, \quad n\to+\infty \tag{38}$$

(this should be opposed to the Hermitian boundary condition $|c_n|\to 1, n\to\pm\infty$ used Sec. III/ B). Obviously, condition (38) is the so-called resonance boundary condition, corresponding to zero amplitude of the incoming wave. In the case of Eq. (36) it is satisfied automatically.

IV. NUMERICAL RESULTS

In this section we describe the numerical procedure used to calculate the scattering matrix, and present some of the numerical results.

A. Quantum resonances

The numerical routine (based on the scientific package MATLAB) is organized in the following way. We write the Hamiltonian $\tilde{H}(t)=(\hat{p}-Ft+\hbar k)^2/2+V(x,t)$ in the exponent of Eq. (16) in the basis of the functions $\langle x|n\rangle$, truncate it to the size $(2N+1)\times(2N+1)$, and calculate the operator exponent as the product of infinitesimal propagators

$$W_N=\prod_{i=1}^{N_t}\exp\left[-\frac{i}{\hbar}\tilde{H}_N(t_i)\Delta t\right], \quad \Delta t=T/N_t, \tag{39}$$

with $N_t\gg 1$. The result is controlled against the variation of N_t. The characteristic structure of the matrix W_N is shown in Fig. 4 for the classical parameters of Fig. 1(a), $\hbar=0.5$ and $N=30$. As expected, the matrix tends to be diagonal in the asymptotic region $|n|>p^*/\hbar$, where $p^*\approx 5$ is the boundary for the chaotic component (see Sec. II). The next stage of the numerical procedure is the construction of the nonunitary matrix B_N [Eq. (21)], which is followed by its diagonalization. To obtain the whole spectrum, the calculation is repeated for every value of k (with the step $\Delta k=1/200$) in the first Brillouin zone.

The resulting complex spectrum is depicted in Fig. 5 in polar coordinates for $q=1$ [Fig. 5(a); see also Fig. 6(b)] and $q=2$ [Fig. 5(b)]. The parameters are $\omega=\frac{10}{6}$, $\epsilon=1.5$, $\hbar=0.25$, $F=q\hbar/T_\omega$, $N=31$, and $N_t=32$. It is seen that the

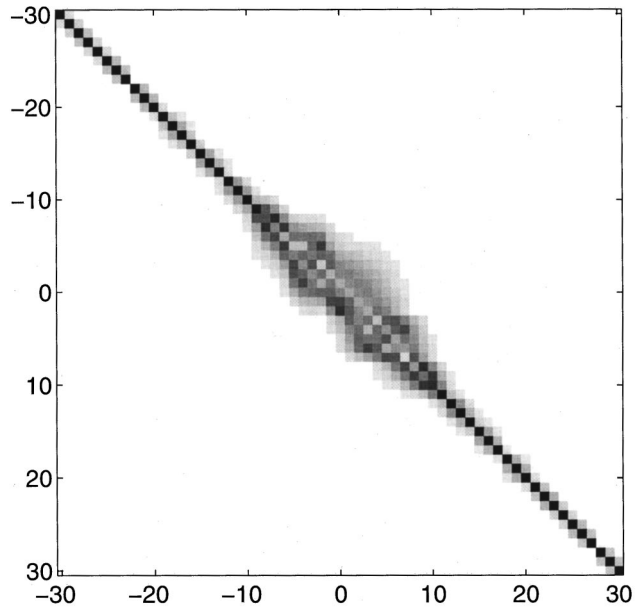

FIG. 4. Characteristic structure of matrix (16). Parameters are $\omega=10/6$, $\epsilon=1.5$, $\hbar=0.5$, and $F=\hbar/T_\omega\approx 0.13$.

spectrum consists of two parts — the resonances associated with the chaotic component (the central part of the matrix W_N) are concentrated close to the unit circle, while the broad resonances associated with outer regular regions (asymptotic part of W_N) are located in the central part of the circle. By increasing N, new such resonances appear in the center. (The positions of the broad resonances already found can be also essentially corrected). These broad resonances are of little physical interest, and we take them out of consideration in the further analysis.

B. Wigner delay time

An important characteristic of the scattering process is the quantity

$$\tau=-\frac{i}{q}\,\frac{d\ln[\det G(\lambda)]}{d\lambda}, \tag{40}$$

which is known in the literature as the Wigner delay time (the quantum analog of the classical delay time), and is directly related to the density of states of a continuous quasienergy spectrum. Another expression for the Wigner delay time has the form

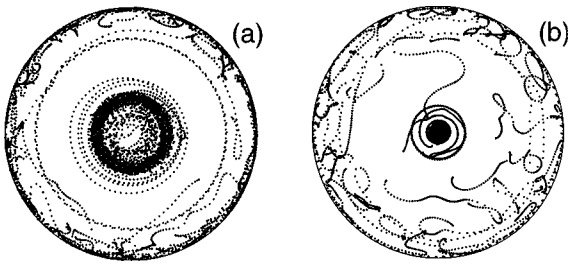

FIG. 5. Complex quasienergy spectrum of the system in (a) the one-channel case $F=\hbar/T_\omega$ and (b) the two-channel case $F=2\hbar/T_\omega$. The quasimomentum k is scanned over the first Brillouin zone with a step $\Delta k=1/200$. The truncation parameter $N=31$.

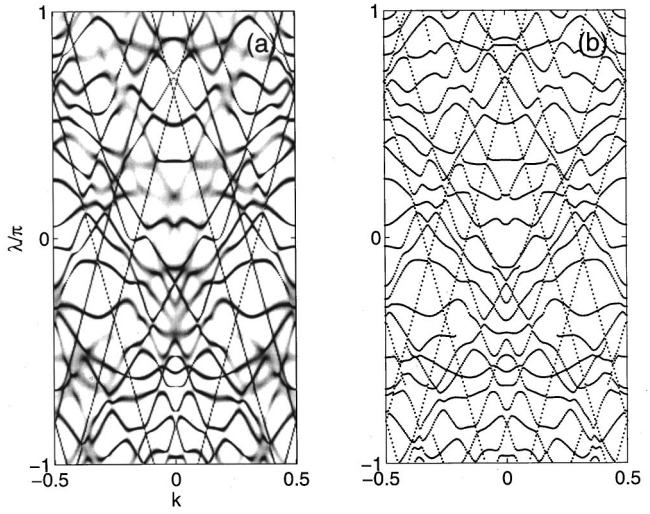

FIG. 6. (a) Delay time $\tau=\tau(\lambda,k)$ in the one-channel case. The limits of the gray-color map are set at $-8\leqslant\tau\leqslant 40$, i.e., the absolute black color corresponds to $\tau>40$, and the white color corresponds to $\tau<-8$. (b) The real part of the complex quasienergy spectrum. Only the 25 most stable states are plotted for each k.

$$\tau=\frac{1}{q}\,\mathrm{Tr}(\hat{\tau}), \tag{41}$$

where

$$\hat{\tau}=-iG^{+}\frac{dG}{d\lambda} \tag{42}$$

is the Smith matrix [19].

A nice feature of the delay time is its stability against an increase of the size of the matrix W_N in Eq. (21). This is due to the fact that the broad resonances (progressively appearing with an increase of N) are located far from the real axis and, therefore, their contribution to the functional dependence $G(\lambda)$, λ real, is negligible. This explains the rapid convergence of the limit in Eq. (23). We also note that the diagonal elements of matrix (42) determine the normalization of the subvector $\mathbf{c}^{(0,i)}$. [The whole vector $\mathbf{c}_\lambda^{(i)}$ is normalized against a δ function: $\langle\mathbf{c}_{\lambda'}^{(i)}|\mathbf{c}_\lambda^{(j)}\rangle=\delta_{i,j}\delta(\lambda'-\lambda)$.] That is,

$$\tau_{i,i}=\lim_{N\to\infty}\sum_{n=-N-q}^{N}(|c_n^{(0,i)}|^2-1/q). \tag{43}$$

A proof of this equation is in line with proving Eq. (35) in Sec. III. A calculation of the delay time τ on the basis of Eqs. (43) and (41) is actually preferable compared to Eq. (40) because it eliminates a numerical estimation of the derivative.

The left panel in Fig. 6 shows the delay time τ as a function of the quasienergy λ and the quasimomentum k for the parameters of Fig. 5(a). In addition, the right panel in Fig. 6 depicts the real part of the complex quasienergies corresponding to the most stable states. As expected, the delay time $\tau=\tau(\lambda,k)$ reveals the underlying resonance structure. For the two-channel case, $q=2$, the Wigner delay time is shown in Fig. 7 together with the proper delay time $\tau_{1,1}$ (a diagonal element of the Smith matrix). It is seen that the

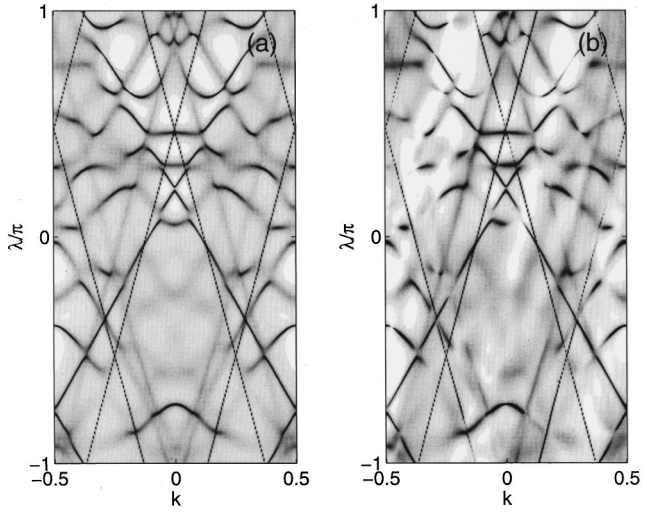

FIG. 7. Delay time in the two-channel case: (a) Wigner delay time $\tau=(\tau_{1,1}+\tau_{2,2})/2$; (b) diagonal element $\tau_{1,1}$ of the Smith matrix.

Wigner delay time is symmetric with respect to an inversion of k, but the proper delay time is not.

To conclude this section we would like to draw the attention of the reader to the regular structure in the straight lines with the slope ± 2 in Figs. 6 and 7, and the circles in Fig. 5. This structure results from the stability islands of classical phase space, and can be determined by using a specific perturbation theory [14]. Apart from this regularity, the structure of the delay times and the complex spectrum looks rather chaotic. In Sec. VI we calculate the distribution functions for the Wigner delay time and the resonance width, and compare them with the prediction of random matrix theory.

V. RANDOM MATRIX APPROACH

A. Hamiltonian based random scattering matrix

We recall some of the results of the random matrix approach to chaotic scattering [3,16,20–22]. Nowadays, the random matrix approach is mainly based on the following definition of a random scattering matrix $S(E)$:

$$S(E)=I-2\pi V^{+}(H_{\mathrm{eff}}-E)^{-1}V, \tag{44}$$

$$H_{\mathrm{eff}}=H-i\pi VV^{+}. \tag{45}$$

In Eqs. (44) and (45) H is an $N\times N$ random matrix belonging to the Gaussian orthogonal ensemble (GOE) or Gaussian unitary ensemble (GUE) universality classes and V is an $N\times M$ coupling matrix satisfying the orthogonality condition

$$\sum_{i=1}^{N} V_{i,a}^{*}V_{i,b}=(g_a/\pi)\,\delta_{a,b}\,.$$

The coupling constants g_a are input parameters of the model. It can be shown that their values define the ensemble averaged diagonal elements of the scattering matrix

$$\langle S_{a,a}(E)\rangle=\frac{1-g_a f(E)}{1+g_a f(E)},\quad f(E)=iE/2+\sqrt{1-E^2/4}, \tag{46}$$

which is an important characteristic in physical applications. [The function $f(E)$ is related to the density of states of system (45), which depends on the energy E).] A matrix of form (44) naturally appears, for example, in the problem of electron scattering in a mesoscopic cavity, [3,20,21]. Then the random Hamiltonian H models N eigenstates of the cavity, and M is number of open channels at the energy E in a lead connecting the cavity with a bath of an electron gas.

Knowing the statistical properties of the Hermitian (symmetric for GOE) matrix in Eq. (44), the distribution for the resonance widths and the distribution for a partial delay time $\tau_i=d\theta_i/dE$ [$\theta_i=\theta_i(E)$ are the eigenphases of the matrix $S(E)$] can be obtained [16]. In the case $N\gg M$, the GUE universality class, and equivalent channels ($g_a=g$) these distributions are

$$P(\tau_s)=\frac{(-1)^M}{M!\,\tau_s^{M+2}}\frac{\partial^M}{\partial(\tau_s^{-1})^M}[\exp(-\kappa\tau_s^{-1})I_0(\tau_s^{-1}\sqrt{\kappa^2-1})] \tag{47}$$

for the scaled partial delay time $\tau_s=\tau\Delta/2\pi$ (Δ is the mean level spacing), and

$$\Pi(\Gamma_s)=\frac{(-1)^M}{(M-1)!}\Gamma_s^{M-1}\frac{d^M}{d\Gamma_s^M}\left(e^{-\kappa\Gamma_s}\frac{\sinh\Gamma_s}{\Gamma_s}\right), \tag{48}$$

for the scaled resonance width $\Gamma_s=\pi\Gamma/\Delta$. In Eqs. (47) and (48), $I_0(z)$ denotes the modified Bessel function and

$$\kappa=\frac{1}{2\mathrm{Re}\,f(E)}(g+g^{-1}), \tag{49}$$

i.e., the distributions are symmetric with respect to $g\to 1/g$.

We also note the relation between the distributions of the resonance width $\Pi(\Gamma_s)$ and distribution $\tilde{P}(\gamma_s)$ of the inverse delay time $\gamma_s=1/\tau_s$

$$\Pi(x)\sim\tilde{P}(x)/x,\quad x\ll 1, \tag{50}$$

which seems to be universal [22]. A remarkable feature of distributions (47) and (48) is the existence of an algebraic tail for both the delay time τ and decay time $\tau'=1/\Gamma$. Physically this means that an electron ''can be captured by the cavity'' for a very long time, if we keep this particular problem in mind.

B. Evolution operator based scattering matrix

One can question whether results (47) and (48) can be applied to our system of interest. In fact, in our case the system Hamiltonian has a ''regular'' structure, and only the evolution operator can be considered as ''random'' in some sense. In addition, the argument of our efficient scattering matrix is a quasienergy (defined in the interval $-\pi<\lambda<\pi$) but not an energy. This would require a random matrix theory of scattering based on the circular ensemble (i.e., an ensemble of random unitary matrices) instead of the Gaussian one. A definition of such a random scattering matrix can be given by using Eqs. (26) and (27), where we just replace the matrix A with a random CUE matrix [23,24].

In the absence of an analytical theory for the statistics of the delay time τ and resonance width Γ of random scattering matrices based on the CUE, we find them numerically. The result is compared with distributions (47) and (48), where we chose $f(E)\equiv 1$ and $\kappa=1$. The reason for this choice of $f(E)$ is that in our case the density of states is uniform [with a mean quasienergy level spacing $\Delta=2\pi/(N-M)$]. The formal reason for the particular choice $\kappa=1$ is the numerical evidence that $\langle G_{a,a}(\lambda)\rangle=0$ [see Eqs. (46) and (49)]. We note that in the case $\kappa=1$, formula (47) simplifies to

$$P(\tau_s)=\frac{1}{M!}\,\frac{1}{\tau_s^{M+2}}\exp\left(-\frac{1}{\tau_s}\right), \tag{51}$$

and the distribution (48) gains quite a specific feature as the power tail for the large resonance width

$$\Pi(\Gamma_s)\sim\frac{M}{2\Gamma_s^2},\quad \Gamma_s\gg 1. \tag{52}$$

Three smooth curves in Fig. 8 show the distribution of the scaled resonance width for the GUE-based scattering matrix for $\kappa=1$ and $M=1,2$, and 3 [see Eq. (48)]. We calculated the distribution of the resonance width for a CUE-based scattering matrix for these three cases and found a perfect coincidence. As an example, in Fig. 8 we depict the histogram for the normalized width $\Gamma\to\pi\Gamma/\Delta=\Gamma(N-M)/2$ for $M=1$. The statistical ensemble involves 5000 CUE matrices of the size $N=41$.

We proceed with the delay time. We find it is more convenient to study the distribution of the diagonal elements $\tau_{i,i}$ of the Smith matrix (42) (the proper delay time) than the distribution of the partial delay time $\tau_i=d\theta_i/d\lambda$. The distributions for these quantities are expected to be essentially the same. We also note the obvious relation

$$\frac{1}{M}\sum_{i=1}^{M}\tau_{i,i}=\frac{1}{M}\sum_{i=1}^{M}\tau_i\equiv\tau,\qquad \tau_i=\frac{d\theta_i}{d\lambda}. \tag{53}$$

Because the proper (partial) delay times are not independent variables, the distribution for the Wigner delay time τ is not a convolution of the distribution for the proper (partial) times. On the contrary, we found that (at least for $M\leqslant 3$) the distribution for the Wigner delay time is close to that of the proper delay time.

The histogram in Fig. 9 shows the distribution $P(\tau)$ of the normalized ($\tau\to\tau\Delta/2\pi=\tau/N$) delay time for $M=1$. This distribution was obtained by generating 50 CUE matrices of the size $N=41$, and calculating $\tau(\lambda)$ for 4000 equal-distant values of λ. The solid line in the figure corresponds to function (51) for $M=1,2$, and 3. A small deviation from the analytical formula is related to a finite matrix size and vanishes with N increased.

The presented numerical results show that the statistics of the delay time and resonance width for random CUE-based scattering matrices [i.e., constructed on the basis of Eqs. (26) and (27)] coincides with the statistics for random GUE-based scattering matrix [Eqs. (44) and (45)] in the case of perfect coupling $\kappa=1$. An analytical proof of this statement appears to be a challenging problem in the field of random matrix theory.

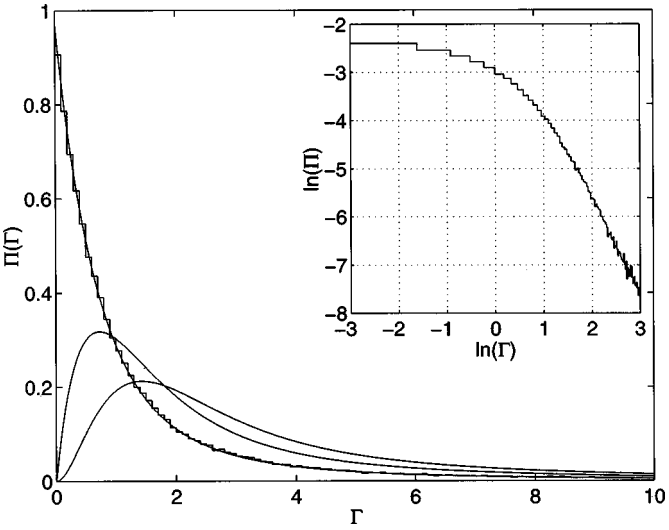

FIG. 8. The histogram shows the distribution of the scaled resonance width for the scattering matrix (26) and (27) with the matrix A belonging to the CUE. The dimension of the matrix A is $N=41$, and the number of channels $M=1$. Solid lines show the distribution [Eq. (48)] for $M=1,2$, and 3, and $\kappa=1$.

VI. COMPARISON WITH RMT

In this section we study the statistics of the resonance width Γ and delay time τ for our deterministic system with Hamiltonian (1). We construct a statistical ensemble by scanning the quasimomentum k with the step Δk over the first Brillouin zone. To have independent representatives of $G(\lambda)$, the step should be of the order of the ''correlation length'' of the quasienergy bands. Decreasing Δk below this characteristic value neither improves nor spoils the statistics. In our numerical calculation we chose $\Delta k=\frac{1}{200}$, which is surely less than the correlation length.

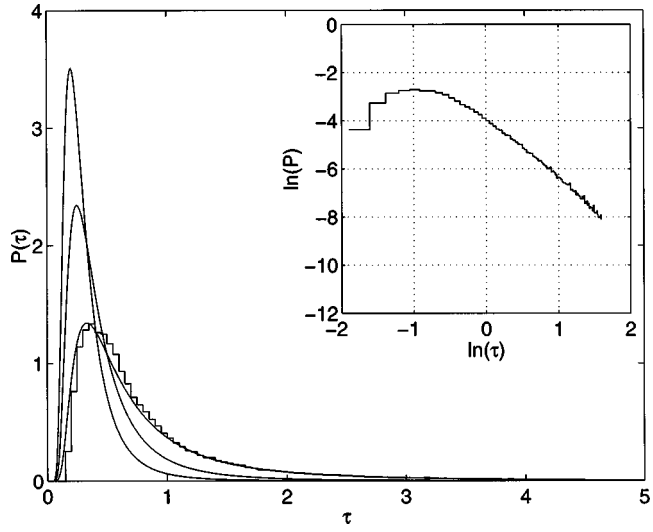

FIG. 9. The same as in the Fig. 8, but for a scaled delay time. The analytical expression is given by Eq. (51).

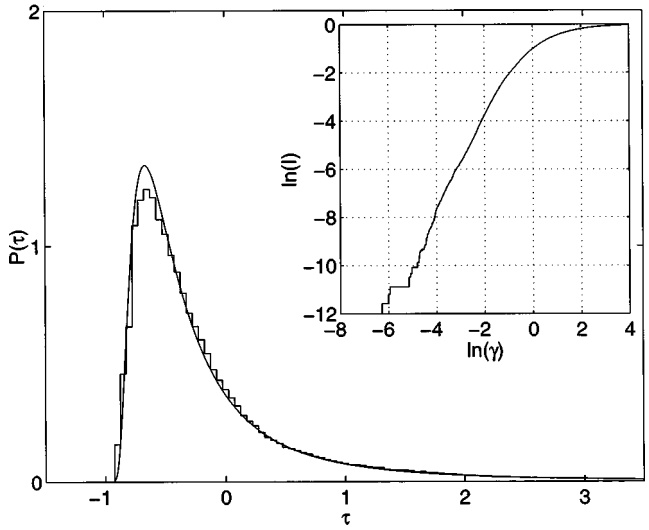

FIG. 10. Distribution of the scaled delay time shown in Fig. 6(a). The inset shows the integrated distribution for the inverse delay time $\gamma=1/\tau$.

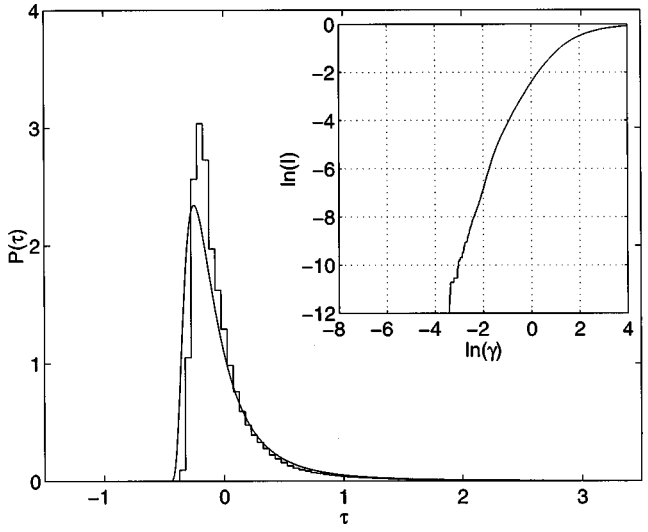

FIG. 11. Distribution of the scaled proper delay time (diagonal element of the Smith matrix) shown in Fig. 7(b).

A. Unitary symmetry

For a fixed value of k, the evolution operator matrix is generally not invariant with respect to inversion of time. Thus we have the case of the unitary symmetry (CUE). Exceptions are the center $k=0$ and the edges $k=\pm 0.5$ of the Brillouin zone, where the time-reversal symmetry is preserved. In principle, the vicinity of these points should be excluded from the consideration. However, in the case of a poor statistical ensemble (i.e., the case we have in hand), this procedure may be neglected. A special precaution should be taken by discretizing the quasienergy λ. In fact, for $\hbar=0.25$ the resonances can be as narrow as $\Gamma\sim 10^{-4}$. Thus, in order not to miss a narrow resonance, the step $\Delta\lambda$ should be small enough. In our calculation we kept $\Delta\lambda=2\pi/4000$.

The main problem one meets by doing the statistics is an appropriate rescaling of the resonance width and delay time. In fact, we cannot directly use the rescaling formulas from Sec. V,

$$\Gamma\to\Gamma(N-M)/2\approx\Gamma N/2, \quad \tau\to\tau/N, \tag{54}$$

because the notion of the matrix size N is not defined for an infinite matrix (16). One notes, however, that the matrix W has a well pronounced structure [see Fig. 4]. Based on this structure, it looks reasonable to choose the ''matrix size'' as

$$N=a/\hbar, \tag{55}$$

where a is an adjusted parameter of the order of $2p^*$. [The physical meaning of quantity (55) is the number of states supported by the chaotic component of the classical phase space, i.e., the volume of the chaotic component per unit cell divided by $2\pi\hbar$.] The other adjusted parameter appears due to the fact that the delay times (43) can be negative for our physical problem (we recall that in the case of RMT, $\tau_{i,i}$ is strictly positive). Thus, to compare with RMT, we should shift the distribution of the scaled delay time by some value $b\approx 1/q$.

Figures 10 and 11 show the distribution of the proper delay time for $q=1$ and 2. [Initial data are displayed in Figs. 6(a) and 7(b), respectively.] The adjusted parameters are $a=7$ and $b=1$ for the one-channel case ($q=1$), and $a=7$ and $b=0.5$ for the two-channel case ($q=2$). The obtained distributions are compared with Eq. (51), where we shifted the analytical curve instead of shifting the histograms. A nice correspondence is noted. To be sure about the asymptotic behavior of $P(\tau)$, we also calculated the integrated distribution $\tilde{P}(\gamma)$ for the inverse delay time $\gamma=1/\tau$ (negative τ were ignored). The result, shown in the inset, coincides with the prediction of RMT:

$$\tilde{P}(\gamma)\sim\gamma^q, \quad I(\gamma)\sim\gamma^{q+1}, \quad \gamma\ll 1. \tag{56}$$

We proceed with the statistics of the resonance width Γ. The initial data are presented in Fig. 5, where we ignore the resonances with $|z|<0.45$. As mentioned above in Sec. IV, these broad resonances are associated with the outer regular region of classical phase space, and cannot be studied by using the RMT approach. The histograms for the scaled resonance width (the adjusted parameter $a=7$ is the same) are shown in Fig. 12 for $q=1$ and Fig. 13 for $q=2$. Unfortunately, the statistics is not well resolved [25]. Nevertheless, one can see the difference between the one and two channel cases, in qualitative agreement with Eq. (48). (A peak around $\Gamma=8$ in Fig. 12 is due to stability islands discussed in the concluding paragraph of Sec. IV.)

B. Antiunitary symmetry

Since the prediction of RMT crucially depends on the global symmetry of the system, it is of interest to study different symmetries of the evolution operator (11). The symmetry of the evolution operator reflects itself in the quasienergy spectrum, and is actually determined by the symmetry of the potential $V(x,t)$ in Hamiltonian (3). Above, we considered the case $V(x,t)=\cos[x-\epsilon\cos(\omega t)]$, where $V(x,-t)=V(x,t)$. In this case the spectrum of the evolution operator is symmetric with respect to the transformation $k\to -k$. In fact, let us present the evolution operator (11) in its k-specific form

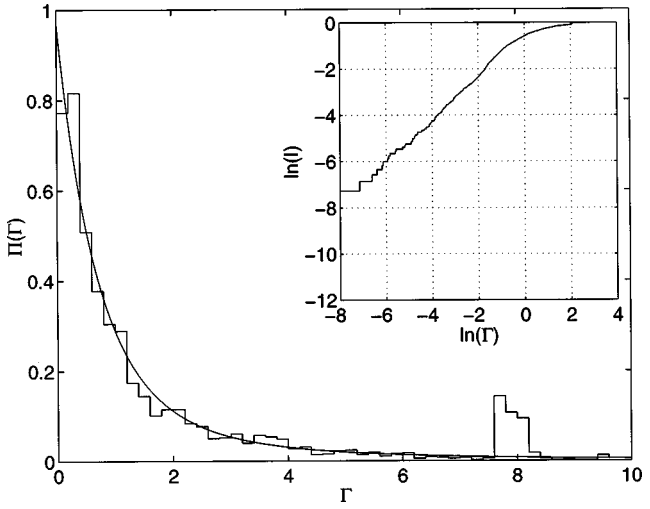

FIG. 12. Distribution of the scaled resonance width in the one-channel case ($q=1$). Data are drawn from Fig. 5(a), where the resonances with $|z|<0.45$ are ignored. The inset shows the integrated distribution.

$$\hat{U}^{(k)}=\exp\left(-i\frac{FT}{\hbar}x\right)\times\widehat{\exp}\left\{-\frac{i}{\hbar}\int_0^T\left[\frac{(\hat{p}+\hbar k-Ft)^2}{2}+V(x,t)\right]\mathrm{d}t\right\}. \tag{57}$$

Applying the time-reversal transformation $R:t\rightarrow -t$, we see that

$$R:\hat{U}^{(k)}=(\hat{U}^{(-k)})^*. \tag{58}$$

Thus the eigenfunction $\chi^{(-k,\lambda)}(x)$ of the operator $\hat{U}^{(-k)}$ is complex conjugate for $\chi^{(k,\lambda)}(x)$, and corresponds to the same quasienergy λ. By noticing that t and k enter Eq. (57) through the combination $\hbar k-Ft$, this symmetry can easily be generalized for $V(x,t)=\cos[x-\epsilon\cos(\omega t+\phi)]$. In this case the point of the mirror symmetry is shifted from $k=0$ to $k=\phi/2\pi$. Excluding the mirror points $k=\phi/2\pi$ and $k=\phi/2\pi+0.5$, this symmetry does not affect the global unitary symmetry and a member of the CUE is an appropriate random matrix for modeling the Floquet operator.

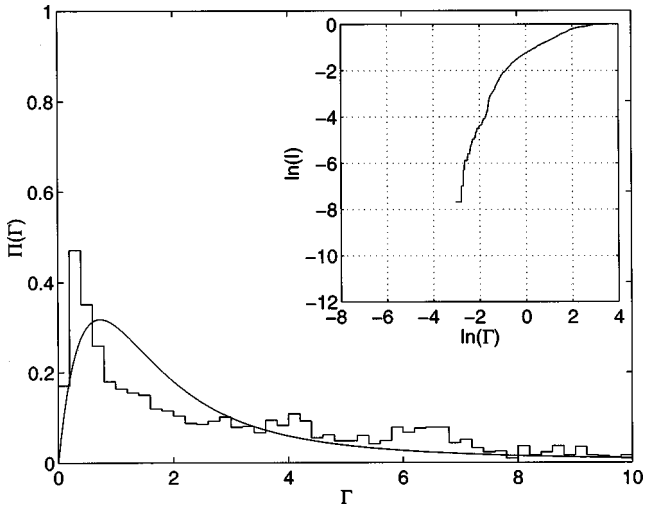

FIG. 13. Distribution of the scaled resonance width in the two-channel case ($q=2$). Data are drawn from Fig. 5(b).

Now we consider the potential $V(x,t)=\cos x\cos(\omega t)$, which effects the unitary symmetry of the evolution operator. In addition to the transformation $t\rightarrow -t$, this potential is also invariant under the transformation $\tilde{R}:x\rightarrow x+\pi,\ t\rightarrow t+T_\omega/2$. This invariance leads to a higher symmetry of the evolution operator. Figure 14 shows the delay time (which characterizes the real continuous spectrum) and the discrete complex quasienergy spectrum (only the real part is shown) for the system with Hamiltonian (7). The parameters are $\omega=0.3$, $\hbar=0.25$, and $F=\hbar/T_\omega$. [For $F=0$ the classical phase portrait of the system is shown in Fig. 1(b).] It is seen that in addition to the symmetry $k\rightarrow -k$, the spectrum is also symmetric with respect to the transformations $k\rightarrow k+0.5$ and $\lambda\rightarrow\lambda+\pi$. Analytically this symmetry is a consequence of the relation

$$\tilde{R}:\hat{U}^{(k)}=e^{i\pi}\hat{U}^{(k+0.5)}. \tag{59}$$

It should be noted that the symmetry equation (59) is *not* a COE symmetry, because the matrix elements of the evolution operator remain complex. However, it changes the statistics in a way similar to that under the transition from unitary to orthogonal symmetry. By analogy with the problem considered in Ref. [26] we shall refer to this symmetry as antiunitary symmetry.

The histogram in Fig. 15 shows the distribution of the delay time depicted in Fig. 14. [The delay time was scaled on the basis of Eq. (55) with $a=3$.] It is seen that this distribution differs essentially from that shown in Fig. 10. We found that now it fits the formula

$$P(\tau_s)=\frac{(1/2)^{1/2}}{\Gamma(1/2)}\frac{1}{\tau_s^{5/2}}\exp\left(-\frac{1}{2\tau_s}\right) \tag{60}$$

[here $\Gamma(x)$ stands for the γ-function] rather well. Equation (60) is a particular case $\beta=1$ of a more general expression

$$P(\tau_s)=\frac{(\beta/2)^{\beta/2}}{\Gamma(\beta/2)}\frac{1}{\tau_s^{(\beta+4)/2}}\exp\left(-\frac{\beta}{2\tau_s}\right) \tag{61}$$

for the distribution of the delay time derived in Ref. [22]. In Eq. (61) $\beta=1,2$, and 4 corresponds to orthogonal, unitary, and symplectic symmetries, respectively, and a one-channel case is assumed. [Note that in the case $\beta=2$ considered above, Eq. (61) coincides with Eq. (51) for $M=1$.]

VII. CONCLUSION

We have studied the scattering of a quantum particle in a dc field by a space- and time-periodic potential. In the case of a static potential (no time dependence) the resonances are arranged in the complex plane in a regular way, forming the so-called Wannier-Stark ladder of resonances. [The corresponding figure for $\lambda(k)$ would consist of straight lines parallel to the k axis, see Fig. 1 in Ref. [12].] In the case of a time-periodic potential the resonance structure is qualitatively different. In this case the classical dynamics of the

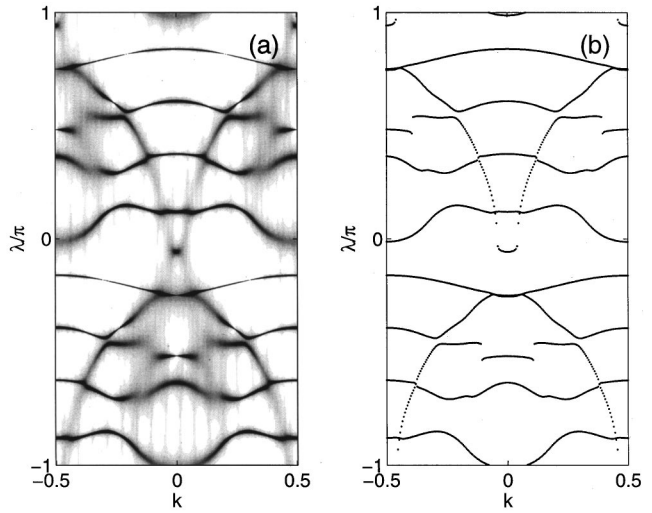

FIG. 14. Delay time as a function of the quasimomentum and quasienergy (a), and the real part of the complex quasienergy spectrum (b) for system (7). The parameters are $\omega=0.3$, $\hbar=0.25$, and $F=\hbar/T_\omega$.

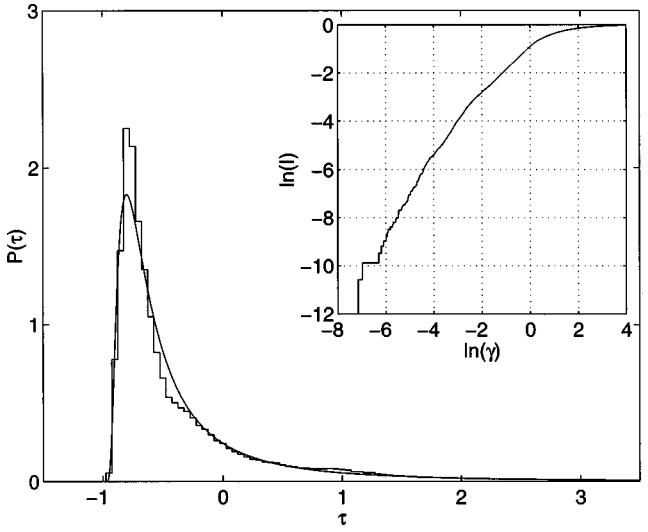

FIG. 15. Distribution of the scaled delay time for system (7) in the one-channel case. The result is compared with Eq. (61).

system is generally chaotic and, as a quantum manifestation of the classical chaos, the location of the resonances is quasirandom. Then a statistical approach should be and has been applied for describing the resonances.

A fundamental conjecture in the field of quantum chaos is that distributions of the different quantities characterizing the quantum resonances (like resonance width or delay time) are universal for a chaotic system, and depend only on its global symmetry. The analytical expressions for these universal distributions are supplied by the random matrix theory of chaotic scattering. The test of our system of interest against the prediction of RMT (and, in reverse, the test of RMT against our physical system) has been the main subject of this paper.

In this paper we restricted ourselves to a calculation of the resonance width and the Wigner delay time. The numerical procedure was based on a method [13] involving the construction of the scattering matrix (23), complex poles of which are the quantum resonances. The calculated resonance widths and delay times were used to find the statistics of these quantities, which is compared with the prediction of RMT given by Eq. (48) for the resonance width, and Eqs. (51) and (61) for the delay time. A striking correspondence was noticed for cases of both unitary ($\beta=2$) and antiunitary ($\beta=1$) symmetries. To our knowledge, this is the first example where data calculated for a real physical system fit so well to the prediction of random matrix theory of chaotic scattering.

ACKNOWLEDGMENT

This research has been supported by the Deutsche Forschungsgemeinschaft (SPP ''Zeitabhängige Phänomene und Methoden in Quantensystemen der Physik und Chemie'' and GK ''Laser und Teilchenspektroskopie'').

[1] U. Smilansky, in *Chaos and Quantum Physics, Proceedings of the Les-Houches Summer School, Session LII*, edited by M. J. Giannoni, A. Voros, and J. Zinn-Justin (North-Holland, Amsterdam, 1991), p. 372.

[2] D. Stone, in *Mesoscopic Quantum Physics, Proceedings of the Les-Houches Summer School, Session LXI*, edited by E. Akkermans, G. Montambaux, and J.-L. Pichard (North-Holland, Amsterdam, 1995), p. 325.

[3] H. A. Weidenmüller, in *Chaos and Quantum Chaos*, edited by W. D. Heiss (Springer, New York, 1992).

[4] E. E. Medez and G. Bastard, Phys. Today **46**(6), 34 (1993).

[5] M. Raizen, C. Solomon, and Qian Niu, Phys. Today **50**(7), 30 (1997).

[6] J. C. Robinson, C. Bharucha, F. L. Moore, R. Jahnke, G. A. Georgakis, Q. Niu, M. G. Raizen, and Bala Sundaram, Phys. Rev. Lett. **74**, 3963 (1995).

[7] F. L. Moore, J. C. Robinson, C. F. Bharucha, Bala Sundaram, and M. Raizen, Phys. Rev. Lett. **75**, 4598 (1995).

[8] K. Vant, G. Ball, H. Ammann, and N. Christensen, Phys. Rev. E (to be published).

[9] D. H. Dunlap and V. M. Kenkre, Phys. Rev. B **34**, 3625 (1986); Nguyen Hong Shon and H. N. Nazareno, J. Phys.: Condens. Matter **4**, L611 (1992); X.-G. Zhao, R. Jahnke, and Q. Niu, Phys. Lett. A **202**, 297 (1995); K. Drese and M. Holthaus, Phys. Rev. Lett. **78**, 2932 (1997).

[10] J. E. Avron and J. Zak, J. Math. Phys. **18**, 918 (1977).

[11] J. E. Avron, Ann. Phys. (N.Y.) **143**, 33 (1982); G. Nenciu, Rev. Mod. Phys. **63**, 91 (1991).

[12] M. Glück, A. R. Kolovsky, H. J. Korsch, and N. Moiseyev, Eur. Phys. J. D **4**, 239 (1998).

[13] M. Glück, A. R. Kolovsky, and H. J. Korsch, Phys. Rev. Lett. **82**, 1534 (1999).

[14] M. Glück, A. R. Kolovsky, and H. J. Korsch, Phys. Rev. E **58**, 6835 (1998).

[15] M. Glück, A. R. Kolovsky, and H. J. Korsch, Phys. Lett. A **249**, 483 (1998).

[16] Y. V. Fyodorov and H. J. Sommers, J. Math. Phys. **38**, 1918 (1997).

[17] A. J. Lichtenberg and M. A. Lieberman, *Regular and Chaotic Dynamics* (Springer, Berlin, 1992); P. J. Bardroff, I. Bialynicki-Birula, D. S. Krämer, G. Kurizki, E. Mayr, P. Stifter, and W. P. Schleich, Phys. Rev. Lett. **74**, 3959 (1995).

[18] We note that system (7) for $F=0$, known as the double resonance model, is one of the chaos paradigms, and has been intensively studied for the last two decades both classically and quantum mechanically (see Ref. [14] for references).

[19] F. T. Smith, Phys. Rev. **118**, 349 (1960).

[20] P. Seba, Phys. Rev. B **53**, 13 024 (1996).

[21] P. Seba, K. Zyczkowski, and J. Zakrzewski, Phys. Rev. E **54**, 2438 (1996).

[22] V. A. Gopar, P. A. Mello, and M. Büttiker, Phys. Rev. Lett. **77**, 3005 (1996).

[23] A random CUE matrix can be easily generated by multiplying the eigenvectors of a GOE matrix (arranged columnwise in a matrix) by a random-phase factor. We use this method in the numerical example presented in this section.

[24] M. Pozniak, K. Zyczkowski, and M. Kus, J. Phys. A **31**, 1059 (1998).

[25] To resolve the statistics one should go to smaller $\hbar$ and F, which would supply more data. Besides this, the limit $\hbar \to 0 F \to 0 (\hbar/F = rT/q)$ corresponds to the $N \to \infty$ limit for the effective size [Eq. (55)] of the Floquet matrix. The latter limit was actually assumed in the analytical expressions given by RMT.

[26] M. V. Berry and M. Robnik, J. Phys. A **19**, 649 (1986); F. M. Izrailev, Phys. Rep. **196**, 299 (1990).